

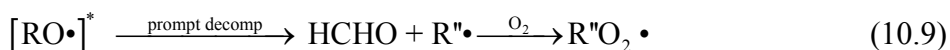
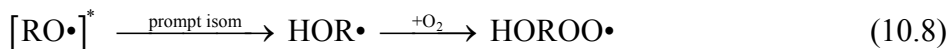
Chapter 10—Cavity Ringdown Spectroscopy and Kinetics of *n*-Butoxy Isomerization: The A-X Electronic Spectrum of HOC₄H₈OO•

Abstract

In Chapters 7 and 8, we have presented the ν_1 spectra of the primary products of alkoxy isomerization (HOR•, HOROO•) and used these absorption bands to measure the relative rate of isomerization to reaction with O₂, $k_{\text{isom}}/k_{\text{O}_2}$. In Chapter 9, we successfully explained the anomalous behavior in the ν_1 absorbance at low [O₂] by showing that the integrated intensities of HOR•, HOROO•, and secondary products differ from each other. Although the spectra in Chapter 7 are relatively clean (93% HOR•, 98% HOROO•), the ideal spectroscopic measurement of HOROO• would come from a clean, unique band free from interference of any secondary products. As we have observed in Chapter 4 (HOCH₂OO•), the A-X spectrum characteristic of all peroxy radicals will satisfy this condition. In this thesis chapter, we present the first detection of the A-X electronic spectrum of the HOC₄H₈OO• radical using cavity ringdown spectroscopy. The spectrum is similar in shape to the A-X spectrum of *n*-butyl peroxy: a broad spectroscopic band due to the multiple molecular conformers that are present. There are two small peaks within this broad band at 7355 and 7556 cm⁻¹, and a shoulder (or possibly a weak peak) at 7500 cm⁻¹. Using the A-X band, we measure the relative absorbance as a function of [O₂] (as in Chapter 8), and obtain $k_{\text{isom}}/k_{\text{O}_2} = (1.39 \pm 0.47) \times 10^{19} \text{ cm}^{-3}$ (2 σ), in good agreement with the ν_1 measurements. Finally, we directly measure the rate of destruction of HOC₄H₈OO•, and determine the kinetic lifetime to be 150 μs in our experiment, in reasonable agreement with our kinetics model.

Introduction

Let us begin with a brief summary of alkoxy radical chemistry and our relative kinetics analysis from Chapters 7–9. In our experiments, thermalized alkoxy radicals ($\text{RO}\cdot$) and hot alkoxy radicals ($[\text{RO}\cdot]^*$) are generated through photolysis of an alkyl nitrite (Reactions 10.1 and 10.2). Once formed, these radicals can undergo isomerization to form a hydroxyalkyl ($\text{HOR}\cdot$, Reaction 10.3), isomerization and rapid association with O_2 to form a hydroxyalkylperoxy ($\text{HOROO}\cdot$, Reaction 10.4), react with O_2 to form HO_2 and an aldehyde (Reaction 10.5), decompose to formaldehyde and an alkyl radical (followed by rapid association to form an alkylperoxy, Reaction 10.6), or recombine with NO to form the alkyl nitrite (Reaction 10.7). Hot alkoxy radicals can promptly isomerize (Reaction 10.8) or decompose (Reaction 10.9).



In Chapter 8, we showed that by measuring the absorbance of a spectroscopic band (A , or A_0 at $[\text{O}_2] = 0$) as a function of $[\text{O}_2]$, we can determine $k_{\text{isom}}/k_{\text{O}_2}$ from Equations 10.10–10.13:

$$\frac{A_0}{A} = \frac{\left(\frac{\frac{k_{\text{O}_2}}{k_{\text{isom}}}}{1 + \frac{k_{\text{NO}}[\text{NO}]}{k_{\text{isom}}} + \frac{k_{\text{decomp}}}{k_{\text{isom}}}} \right) [\text{O}_2] + 1}{\left(\frac{\phi_{\text{pi}} \frac{k_{\text{O}_2}}{k_{\text{isom}}}}{1 + \phi_{\text{pi}} \left(\frac{k_{\text{NO}}[\text{NO}]}{k_{\text{isom}}} + \frac{k_{\text{decomp}}}{k_{\text{isom}}} \right)} \right) [\text{O}_2] + 1}, \quad (10.10)$$

$$\frac{k_{\text{isom}}}{k_{\text{O}_2}} = \left[\left(\frac{\partial \left(\frac{A_0}{A} \right)}{\partial [\text{O}_2]} \right)_{[\text{O}_2]=0} \right]^{-1} \times X_{\text{kin}} \times X_{\text{prompt}}, \quad (10.11)$$

where

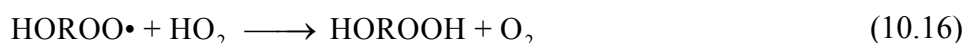
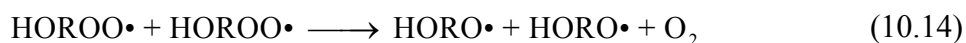
$$X_{\text{kin}} = \frac{1}{1 + \frac{k_{\text{decomp}}}{k_{\text{isom}}} + \frac{k_{\text{NO}}[\text{NO}]}{k_{\text{isom}}}}, \quad (10.12)$$

$$X_{\text{prompt}} = \frac{(1 - \phi_{\text{pi}})}{1 + \phi_{\text{pi}} \left(\frac{k_{\text{decomp}}}{k_{\text{isom}}} + \frac{k_{\text{NO}}[\text{NO}]}{k_{\text{isom}}} \right)}. \quad (10.13)$$

One possible problem with using the ν_1 band is that it is not a truly unique measure of HOROO•. In Chapter 9, we showed that secondary products formed in appreciable quantities over timescales of even 100 μs . These products do not necessarily have the same absorption cross section as HOROO•. The effect of these secondary products is likely minimal due to two observations: 1) the ν_1 absorbance is constant over

1 ms (Chapter 7), and 2) the simulation of relative kinetics (Chapter 9) is in excellent agreement with our CRDS data (Chapter 8).

Nonetheless, measurement of a spectroscopic band unique to HOROO• presents many benefits. First, the problem of varying absorption cross sections as a function of [O₂] disappears, eliminating one possible confounding factor in our analysis of $k_{\text{isom}}/k_{\text{O}_2}$. Second, and perhaps more importantly, direct kinetics measurements can be made on HOROO•. We have already shown in Chapter 7 that measuring the formation of HOROO• is not possible at room temperature because the isomerization lifetime (5 μs) is on the same order as our ringdown lifetime (7 μs). On the other hand, destruction of HOROO• is expected to take place on much longer timescales (lifetimes > 100 μs), and measuring this should be possible, with the major destruction pathways being self-reaction (Reaction 10.14, $k = 5 \times 10^{-13} \text{ cm}^3 \text{ molec}^{-1} \text{ s}^{-1}$), reaction with NO (Reaction 10.15, $k = 9 \times 10^{-12} \text{ cm}^3 \text{ molec}^{-1} \text{ s}^{-1}$), and reaction with HO₂ (Reaction 10.16, $k = 8 \times 10^{-12} \text{ cm}^3 \text{ molec}^{-1} \text{ s}^{-1}$).^{27, 117, 118} Under most experimental conditions ([O₂] < 1 atm), the NO destruction pathway should dominate, underscoring the need to obtain a reasonably accurate [NO], notably the NO present in the *n*-butyl nitrite sample.



As stated in Chapter 4, hydroxyalkylperoxy molecules have distinct A-X electronic spectra, similar in shape and position to the corresponding alkylperoxy spectra. It is therefore expected that HOROO• will have a similar A-X spectrum to the corresponding ROO•. As a starting point, the smallest possible alkoxy isomerization

product, δ -HOC₄H₈OO•, will have a similar A-X spectrum to *n*-butylperoxy:¹⁹⁰ a broad band over 7200–7700 cm⁻¹ with two or three small peaks. The decomposition of C₄H₉O• is slow (lifetime 2 ms), and Mollner³⁰ and Sprague³¹ have shown that the prompt decomposition yield (Reaction 10.9) following 351 nm photolysis of *n*-butyl nitrite is less than 5%. Therefore, on short timescales, we expect to only observe the A-X transition of HOC₄H₈OO•, and not the decomposition product C₃H₇OO•.

This thesis chapter describes the first detection of the A-X electronic band of HOC₄H₈OO•, direct kinetics measurements on the destruction of HOC₄H₈OO•, determination of the relative kinetic rate constants $k_{\text{isom}}/k_{\text{O}_2}$ for *n*-butoxy using this spectroscopic band, and FTIR experiments to determine [NO] in the *n*-butyl nitrite used to generate the butoxy radicals. Similar to the experiments in Chapters 7 and 8, HOC₄H₈OO• was generated through pulsed laser photolysis of *n*-butyl nitrite in the presence of O₂. Cavity ringdown spectroscopy was used to measure the resulting spectrum over the range 7150–7700 cm⁻¹, 10 μs after photolysis. The resulting peak heights were measured over the first 500 μs after photolysis in order to assess the rate of destruction of HOC₄H₈OO•. The A-X peak heights were measured as a function of [O₂] to obtain $k_{\text{isom}}/k_{\text{O}_2}$. FTIR spectra of *n*-butyl nitrite were taken before and after purification (freeze-pump-thaw cycles) to determine the presence and nature of contaminants in our cavity ringdown experiments.

Methods

Apparatus and Chemicals

The cavity ringdown spectrometer, laser system, and gas kinetics flow cell have been described in detail in Chapter 2 (Figures 2.5, 2.7, 2.8). Briefly, the tunable near-infrared light used to measure the spectrum ($6900\text{--}7800\text{ cm}^{-1}$, $100\text{ }\mu\text{J/pulse}$) was generated by sending the output from a Nd:YAG (532 nm, 370 mJ/pulse, 10 Hz) pumped dye laser (DCM dye, 620–660 nm, 35 mJ/pulse peak) into a H₂ filled Raman shifter. The infrared light was sent into an optical cavity consisting of two highly reflective mirrors (Los Gatos Research, 1.35 μm peak, R = 99.98%). Ringdown traces were collected with an amplified InGaAs detector (ThorLabs PDA400 or PDA10CS) connected to a PC oscilloscope card (GageScope CS1450). 80 μs of ringdown data were collected per shot, and 16 ringdowns were collected and averaged before being fit. The first eighth of the ringdown lifetime was removed before the data were refit in order to eliminate errors caused from noise near the peak of the ringdown.

$\delta\text{-HOC}_4\text{H}_8\text{OO}\cdot$ radicals were formed by photolysis of *n*-butyl nitrite (95%, Sigma-Aldrich) in the presence of O₂ (Reactions 10.1 and 10.4). Photolysis was initiated by 351 nm light from the excimer laser described in Chapter 2. Typical UV flux was kept at 2.5×10^{17} photons cm^{-2} . The absorption cross section of *n*-butyl nitrite at 351 nm is $\sigma_{351\text{nm}} = 8.0 \times 10^{-20}$ $\text{cm}^2\text{ molec}^{-1}$,³² resulting in 2.0% of the alkyl nitrite being photolyzed.

n-butyl nitrite was introduced to the gas kinetics cell by flowing N₂ gas through a bubbler kept at 0 °C. Prior to usage, the *n*-butyl nitrite went through a minimum of three freeze-pump-thaw cycles in order to degas the sample of oxygen and to reduce the concentration of impurities (such as NO, nitrous oxides, aldehydes, and acids). Briefly,

one cycle consists of freezing the nitrite in liquid nitrogen, vacuum pumping on the sample for 10–20 minutes, then isolating the sample and thawing. The gas bubbles that evolve represent impurities that have a higher vapor pressure than the nitrite. Cycles were repeated until minimal to no gas evolved during thawing.

Experimental and Flow Conditions

Four experiments were conducted on the *n*-butoxy chemical system. First, the A-X electronic spectrum of $\text{HOC}_4\text{H}_8\text{OO}\cdot$ was measured by scanning across a range of frequencies ($7150\text{--}7700\text{ cm}^{-1}$, step size 1 cm^{-1}) while at a constant time after photolysis of the *n*-butyl nitrite ($10\text{ }\mu\text{s}$). Second, the A-X band was used to directly measure the rate of destruction of $\text{HOC}_4\text{H}_8\text{OO}\cdot$ by keeping the laser at one frequency (7556 cm^{-1}) and measuring the change in absorption with time after photolysis of the *n*-butyl nitrite ($0\text{--}400\text{ }\mu\text{s}$). Although these two experiments were conducted at two different pressures (670 and 330 torr), one set of common chemical concentrations was used to show that the destruction of $\text{HOC}_4\text{H}_8\text{OO}\cdot$ is pressure independent. This experiment was repeated for two different values of $[\text{C}_4\text{H}_9\text{ONO}]$ (3.4×10^{16} and $1.6 \times 10^{16}\text{ molec cm}^{-3}$) and three different values of photolysis ratio (2.0% , 1.0% , 2.8%), for a total of six experimental conditions. Third, the relative rate constant $k_{\text{isom}}/k_{\text{O}_2}$ was measured by varying $[\text{O}_2]$, $(0\text{--}8) \times 10^{18}\text{ molec cm}^{-3}$ at constant pressure (330 torr) and measuring the resulting absorption at a constant frequency (7556 cm^{-1}) and time after photolysis ($10\text{ }\mu\text{s}$).

The conditions for the three experiments are summarized in Table 10.1. Gas flows were measured using the flowmeters discussed in Chapter 2. The temperature of the gas

kinetics cell was taken to be room temperature: no temperature control of any kind was attempted.

Table 10.1. Experimental conditions (gas flows, photolysis parameters, chemical concentrations, and spectrometer performance) for alkoxy experiments

	Spectrum and direct kinetics, 670 torr	Spectrum and direct kinetics, 330 torr	Relative rate, 330 torr
N ₂ Purge Flow—Left Mirror	700 sccm	650 sccm	650 sccm
N ₂ Purge Flow—Right Mirror	900 sccm	450 sccm	450 sccm
N ₂ Bubbler Flow	250 sccm	250 sccm 125 sccm ^b	225 sccm
N ₂ Dilution Flow	6500 sccm	2900 sccm	0–2900 sccm ^a
O ₂ Flow	70 sccm	70 sccm	0–2900 sccm ^a
Cell Pressure	670 torr	330 torr	330 torr
Temperature (room)	293 ± 2 K	293 ± 2 K	293 ± 2 K
Flush Time	57 ms	28 ms	28 ms
Photolysis Window Length	5 cm	5 cm	5 cm
Excimer Energy at 351 nm	162 ± 10 mJ/pulse	162 ± 10 mJ/pulse 84 ± 5 mJ/pulse ^b 240 ± 15 mJ/pulse ^b	162 ± 10 mJ/pulse
% Alkoxy Photolyzed	1.98%	1.98% 0.95% ^b 2.83% ^b	1.98%
[C ₄ H ₉ ONO] _{cell}	3.4 × 10 ¹⁶ cm ⁻³	3.4 × 10 ¹⁶ cm ⁻³ 1.6 × 10 ¹⁶ cm ⁻³ ^b	3.4 × 10 ¹⁶ cm ⁻³
[C ₄ H ₉ O•]	6.5 × 10 ¹⁴ cm ⁻³	6.5 × 10 ¹⁴ cm ⁻³ 3.2 × 10 ¹⁴ cm ⁻³ ^b 9.1 × 10 ¹⁴ cm ⁻³ ^b 1.6 × 10 ¹⁴ cm ⁻³ ^b 4.6 × 10 ¹⁴ cm ⁻³ ^b	6.5 × 10 ¹⁴ cm ⁻³
[O ₂]	2.0 × 10 ¹⁷ cm ⁻³	2.0 × 10 ¹⁷ cm ⁻³	0–8 × 10 ¹⁸ cm ⁻³
Optical Cell Length	52 cm	52 cm	52 cm
1/τ ₀ (7500 cm ⁻¹ , vacuum)	1.1 × 10 ⁵ Hz	1.2 × 10 ⁵ Hz	0.9 × 10 ⁵ Hz
1/τ (7500 cm ⁻¹ , all gases and C ₄ H ₉ ONO)	1.3 × 10 ⁵ Hz	1.3 × 10 ⁵ Hz	0.9 × 10 ⁵ Hz
Δτ/τ ^c	0.7%	0.7%	0.7%
Sensitivity, 7500 cm ⁻¹	2.0 ppm Hz ^{-1/2}	2.0 ppm Hz ^{-1/2}	1.4 ppm Hz ^{-1/2}

a) The sum of O₂ and N₂ dilution flows was kept at 2900 sccm for the relative rate experiments to keep a constant pressure and flush time

b) Excimer flux and concentrations used only for direct kinetics measurements

c) Δτ/τ reported for averaging 16 ringdown traces per point

The cell flush time, [RONO], and [RO•] are calculated from the experimental parameters Table 10.1. Derivations of these equations were presented in Chapter 8; therefore, only the final results are presented here. The flush time is defined as the amount of time to remove the chemicals within the photolysis length from the ringdown cavity, and is calculated from Equation 10.17:

$$t_{flush} = \left(\frac{V_{in-out}}{\sum_{flush} f_i} \right) \times \left(\frac{p_{cell}}{p_{st}} \right), \quad (10.17)$$

where t_{flush} is the flush time for the chemical sample, V_{in-out} is the volume between the inlet for butyl nitrite and vacuum outlet ($V_{in-out} = 3.93 \text{ cm}^3$ for the cell used in this experiment), $\sum_{flush} f_i$ is the total flow rate of gases in the direction of flushing (in sccm), p_{cell} is the pressure in the CRDS cell, and p_{st} is the standard pressure (760 torr).

[RONO] in the CRDS cell is determined by the vapor pressure of the alkyl nitrite and the dilution of the butyl nitrite carrier gas within the CRDS cell, and can be calculated from Equation 10.18:

$$\left(\frac{N}{V} \right)_{RONO,CRDS} = p_{vap} \left(\frac{N/V}{p} \right)_{conv} \left(\frac{T_{bubbler}}{T_{cell}} \right) \left(\frac{f_{bubbler}}{\sum f_i} \right), \quad (10.18)$$

where $\left(\frac{N}{V} \right)_{RONO,CRDS}$ is the concentration of butyl nitrite in the CRDS cell, p_{vap} is the vapor pressure of RONO in the bubbler, $T_{bubbler}$ is the temperature of the bubbler (273 K),

$\left(\frac{N/V}{p} \right)_{conv}$ is the conversion factor between pressure and number density of a gas

$(3.24 \times 10^{16} \text{ molec cm}^{-3}/\text{torr})$, T_{cell} is the temperature of the gas kinetics cell (293 K), f_{bubbler} is the gas flow through the bubbler, and Σf_i is the sum of all gas flows through the gas kinetics cell. The vapor pressure of $\text{C}_4\text{H}_9\text{ONO}$ (20.3 torr at 273 K) can be computed based on known thermodynamic properties (ΔH_{vap} , $T_{\text{boil,1atm}}$).

The fraction of RONO that is photolyzed can be calculated from Equation 10.19:

$$\%_{\text{photolysis}} = \frac{\left(\frac{P_{\text{excimer}}}{A_{\text{meter}}} \right)}{F_{\text{excimer}}} \left(\frac{\lambda}{hc} \right) (\sigma_{\text{RONO},\lambda}) (X) \left(\frac{A_{\text{UV,laser}}}{A_{\text{UV,CRDS}}} \right), \quad (10.19)$$

where $\%_{\text{photolysis}}$ is the fraction of RONO that is photolyzed, $(P_{\text{excimer}}/A_{\text{meter}})$ is the power per unit area of the UV light (read directly from the power meter), F_{excimer} is the rep rate of the excimer laser (10 Hz), h is Planck's constant, c is the speed of light, λ is the wavelength of the excimer light (351 nm), $\sigma_{\text{RONO},\lambda}$ is the absorption cross section of RONO at the excimer wavelength ($8 \times 10^{-20} \text{ cm}^2 \text{ molec}^{-1}$ at 351 nm for *n*-butyl nitrite), X is the quantum yield for photolysis (taken to be 1), $A_{\text{UV,laser}}$ is the area of excimer beam measured at the excimer laser output, and $A_{\text{UV,CRDS}}$ is the area of excimer beam measured at the CRDS cell. For these experiments, $\frac{A_{\text{UV,laser}}}{A_{\text{UV,CRDS}}} = 2$.

FTIR—Apparatus, Chemicals, Methods

Gas phase FTIR spectra of *n*-butyl nitrite (95%, Sigma-Aldrich) were acquired using the Nicolet FTIR instrument in Paul Wennberg's lab (path length 19 cm). The nitrite samples were placed in a flask and atmospheric gas was pumped off (freezing the nitrite, pumping off gas for 1 minute, then thawing the nitrite) before use. The vapor from the butyl nitrite was sent into the FTIR cell: no gas was bubbled through the liquid

sample. Butyl nitrite samples were injected and pumped out of the FTIR three times before the gas to be measured was injected to ensure that no residual air was present in the FTIR.

Four different *n*-butyl nitrite samples were measured to assess how purification, storage, and sample age affect nitrite purity. The four samples that were measured were freshly purchased nitrite that was freeze pumped, freshly purchased nitrite that was not freeze pumped, 4-week-old nitrite stored at 4 °C that was not freeze pumped, and 8-week-old nitrite stored at room temperature that was not freeze pumped. The pressure of the nitrite vapor in the FTIR was measured using a Baratron (MKS). The experimental conditions for each sample are summarized in Table 10.2.

Table 10.2. Experimental conditions for FTIR spectra of butyl nitrite samples

	Units	1	1a	1b	2	2a	3	4
Sample Age		Fresh	Fresh	Fresh	Fresh	Fresh	4 wks	8 wks
Storage Temp	K	277	277	277	277	277	277	293
Freeze Pump?		yes	yes	yes	no	no	no	no
Pressure	torr	148	62	77	68	66	65	65

The FTIR spectra were compared to reference spectra⁴⁰ of NO and C₂H₅ONO to determine the purity of the butyl nitrite, similar to the methods of assessing our 2-pentyl nitrite in Chapter 7. The resulting concentrations were used to calculate [NO] in the CRDS experiment.

Results

We present the results of this study in four parts. First, the A-X spectrum of HOC₄H₈OO• is reported. The spectrum is similar in shape to the literature spectrum of C₄H₉OO•:¹⁹⁰ a broad absorption band over the range 7200–7700 cm⁻¹ with two small

peaks. Second, the kinetics of $\text{HOC}_4\text{H}_8\text{OO}\cdot$ destruction are reported by using the A-X spectroscopic band for six combinations of $[\text{C}_4\text{H}_9\text{ONO}]$ and photolysis ratios. In all cases, the lifetime of $\text{HOC}_4\text{H}_8\text{OO}\cdot$ is 150 μs , in reasonable agreement with our kinetics model. Third, the relative rate $k_{\text{isom}}/k_{\text{O}_2}$ is reported by using the A-X spectroscopic band to obtain A_0/A as a function of $[\text{O}_2]$. The relative rate obtained with the A-X band is in agreement with all of the previous literature studies, including our OH stretch CRDS measurements (Chapter 8). This result gives us further confidence in assigning the measured NIR spectrum to $\text{HOC}_4\text{H}_8\text{OO}\cdot$. Fourth, the FTIR spectra of the *n*-butyl nitrite samples are presented, and the amount of NO present in the CRDS experiments is calculated. We calculate a small but observable amount of NO that comes from the *n*-butyl nitrite sample.

A-X Spectrum of $\text{HOC}_4\text{H}_8\text{OO}\cdot$

Figure 10.1 shows the A-X spectrum of $\text{HOC}_4\text{H}_8\text{OO}\cdot$. This spectrum was taken 10 μs after photolysis of *n*-butyl nitrite, over the range 7150–7700 cm^{-1} , with a step size of 1 cm^{-1} . Background water absorptions increase the noise in the spectrum, rendering some of the scans across the region 7150–7400 cm^{-1} unusable. Therefore, two regions of the spectrum have different amounts of averaging per point. Each point in the range 7150–7400 cm^{-1} has 6.4 s of averaging (4 scans), while each point in the range 7400–7700 cm^{-1} has 24 s of averaging (15 scans). The spectrum inset in the upper right corner is the A-X cavity ringdown spectrum of *n*-butylperoxy obtained by Glover and Miller.¹⁹⁰

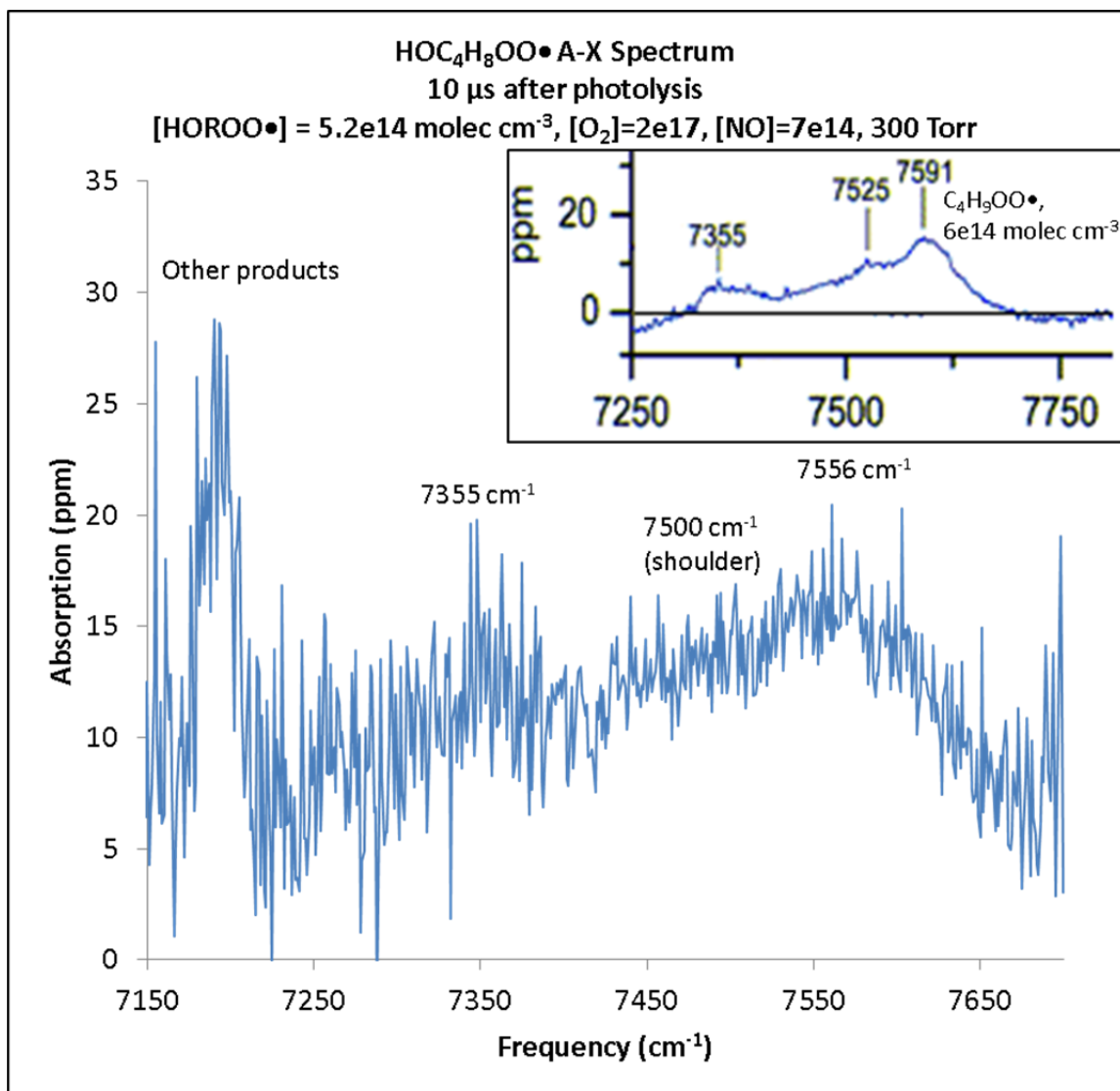


Figure 10.1. Cavity ringdown spectrum of the A-X electronic transition for the δ -hydroxybutylperoxy radical (HOC₄H₈OO•). A broad absorption is observed over the range 7200–7700 cm⁻¹, with two peaks at 7355 and 7556 cm⁻¹. A shoulder is also present at 7500 cm⁻¹. These three features are similar in position and intensity to the three peaks found in the spectrum of *n*-butylperoxy, inset in the upper right corner for reference.¹⁹⁰ The peak at 7190 cm⁻¹ is assigned to other, stable, photolysis products. Inset spectrum adapted with permission from Glover *et al.*¹⁹⁰ Copyright 2005 American Chemical Society.

There are a few features of the A-X spectrum of HOC₄H₈OO• to note. We observe a broad absorption over the range 7200–7700 cm⁻¹, with two peaks (7355 cm⁻¹, 12 ppm; and 7556 cm⁻¹, 16 ppm) and a shoulder (centered at 7500 cm⁻¹; 13 ppm). No

rotational lines can be observed (in contrast to the spectrum of HOCH₂OO• presented in Chapter 4) due to the large number of molecular conformers present. As observed in other alkyl peroxy studies,^{184, 190, 195} a large absorption at 7190 cm⁻¹ is observed. This peak is attributed to stable photolysis products, and not to alkyl peroxies, including HOC₄H₈OO•. This can be confirmed by examination of the kinetics of this peak, presented later in this chapter.

A comparison of the spectrum of HOC₄H₈OO• to Glover and Miller's spectrum of C₄H₉OO• shows that both peroxies have very similar spectral features. Both spectra have three similar features in very similar regions. The spectrum of HOC₄H₈OO• has a small broad peak at 7355 cm⁻¹, a shoulder at 7500 cm⁻¹, and a large broad peak at 7556 cm⁻¹. Similarly, the spectrum of C₄H₉OO• has a small broad peak at 7355 cm⁻¹, a very weak peak/shoulder at 7525 cm⁻¹, and a larger broad peak at 7591 cm⁻¹. The small shifts in peak positions are likely due to energy shifts in the valence orbitals from interactions between the OH and OO• groups, similar to the HOCH₂OO• vs CH₃OO• transition frequencies presented in Chapter 5.

Finally, the peak intensities and relative intensities are summarized in Table 10.3. We note similar absolute absorbances. Our kinetics model (presented later in the *Kinetics* section) predicts that we will form [HORO•] = 5×10^{14} molec cm⁻³, and that 99% of the chemical species with a peroxy group in the system are HOROO•. Glover and Miller's A-X spectrum of C₄H₉OO• was taken by photolysis of C₄H₉I in the presence of O₂.¹⁹⁰ Typical C₄H₉• formed was 6×10^{14} molec cm⁻³, with no estimate of how much was converted to C₄H₉OO•. Still, we expect Glover's [C₄H₉OO•] to be approximately equal to our [HOC₄H₈OO•] (within a factor of 2), and our absorbance data support this.

Table 10.3. Absolute and relative absorbances for the A-X peaks in δ -HOC₄H₈OO• and *n*-C₄H₉OO•.

	A_{7355}^a	A_{7500}^a	A_{7550}^a	A_{7500}/A_{7355}	A_{7550}/A_{7355}	A_{7550}/A_{7500}
δ -HOC ₄ H ₈ OO•	12	13	16	1.1	1.3	1.2
<i>n</i> -C ₄ H ₉ OO•	6	10	14	1.7	2.3	1.4

a) Absorbances in ppm

We also note that the relative intensities of the three features differ between the two spectra. In our δ -HOC₄H₈OO• spectrum, the absorption at 7355 cm⁻¹ is nearly as strong as the other two features. In contrast, the 7355 cm⁻¹ absorption in *n*-C₄H₉OO• is a factor of 2 weaker than the other two features.¹⁹⁰ This could be explained in a number of ways: different conformers being populated for each molecule, different Franck-Condon factors, or different dipole-derivatives. It would be interesting and worthwhile to examine this behavior in detail with a quantum chemistry study similar to the one in Chapter 5.

Kinetics

One of the major benefits of measuring the A-X band is that we can measure the kinetics of HOC₄H₈OO• destruction. Figure 10.2 shows six plots of the A-X absorbance (7556 cm⁻¹) as a function of time after RONO photolysis. A combination of two [RONO] (3.4×10^{16} molec cm⁻³ and 1.4×10^{16} molec cm⁻³) and three photolysis ratios (2.83%, 1.98%, 0.95%) gave rise to six different experimental conditions, allowing us to observe whether the kinetics were affected by [RO•] or [RONO]. For all scans, [O₂] = 2×10^{17} molec cm⁻³. The HOC₄H₈OO• lifetimes (1/e time for absorbance) were calculated by drawing an average line through the kinetics data, and are summarized in Table 10.4. The large noise level in each kinetics plot causes our lifetime estimates to have at least 20% error.

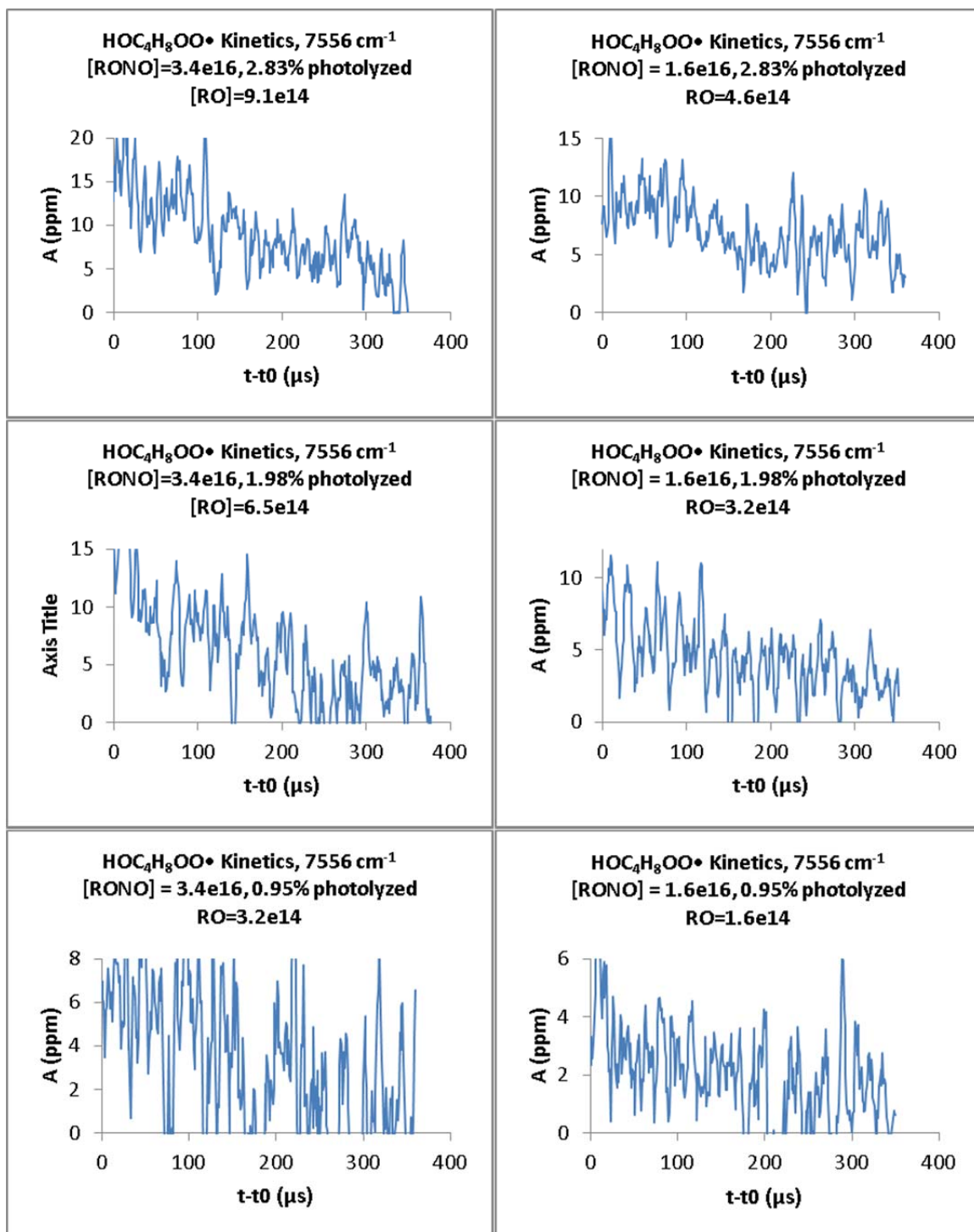


Figure 10.2. Direct kinetics measurements of $\text{HOC}_4\text{H}_8\text{OO}\cdot$ via the A-X band (7556 cm^{-1}), 0–350 μs after $\text{C}_4\text{H}_9\text{O}\cdot$ formation. Various $[\text{RONO}]$ and photolysis ratios were used (see individual plots for details). For all experiments, $[\text{O}_2] = 2 \times 10^{17}\text{ molec cm}^{-3}$, $p = 300\text{ torr}$. The low $[\text{RO}\cdot]$ experiments give rise to low $[\text{HOROO}\cdot]$, and therefore noisy kinetics data, making interpretation of the data difficult. The lifetimes of $\text{HOROO}\cdot$ are on the order 200–400 μs , and are summarized in Table 10.4.

Table 10.4. Observed and modeled $\text{HOC}_4\text{H}_8\text{OO}\cdot$ lifetimes ($1/e$ time), $[\text{O}_2] = 2 \times 10^{17}$ molec cm^{-3} , $p = 300$ torr.

[RONO] (molec cm^{-3})	[RO•] (molec cm^{-3})	[NO] ^a (molec cm^{-3})	$\tau_{\text{HORO}\cdot}$ obs. (μs)	$\tau_{\text{HORO}\cdot}$ model (μs)
3.4×10^{16}	9.1×10^{14}	9.6×10^{14}	200	170
3.4×10^{16}	6.5×10^{14}	7.0×10^{14}	200	250
3.4×10^{16}	3.2×10^{14}	3.7×10^{14}	275	450
1.6×10^{16}	4.6×10^{14}	4.8×10^{14}	300	310
1.6×10^{16}	3.2×10^{14}	3.4×10^{14}	300	425
1.6×10^{16}	1.6×10^{14}	1.8×10^{14}	>350	>500

a) Assumes RONO:NO=700:1 in sample

b) Error on observed lifetimes is at least $\pm 20\%$

We observe lifetimes of $\text{HORO}\cdot$ on the order of 200–400 μs . The lifetime increases as we reduce radical concentrations (RO• or NO). These compare favorably to the lifetimes obtained from our kinetics simulations, summarized in the final column. We conclude that the secondary chemistry of $\text{HORO}\cdot$ is reasonably well modeled.

Kinetics simulations are shown in Figure 10.3 for $\text{HOC}_4\text{H}_8\text{OO}\cdot$ and other peroxies under our experimental conditions. At 500 μs , we observe formation of $\text{C}_4\text{H}_9\text{OO}\cdot$ (up to 25% of the $\text{HOC}_4\text{H}_8\text{OO}\cdot$ concentration). At these times, we expect two contributions to the A-X spectrum and our measured kinetics in Figure 10.2: $\text{HOC}_4\text{H}_8\text{OO}\cdot$ (major product) and $\text{C}_4\text{H}_9\text{OO}\cdot$ (minor product). Formation of additional peroxies implies that we cannot make meaningful kinetics measurements of $\text{HOC}_4\text{H}_8\text{OO}\cdot$ at long times ($>500 \mu\text{s}$).

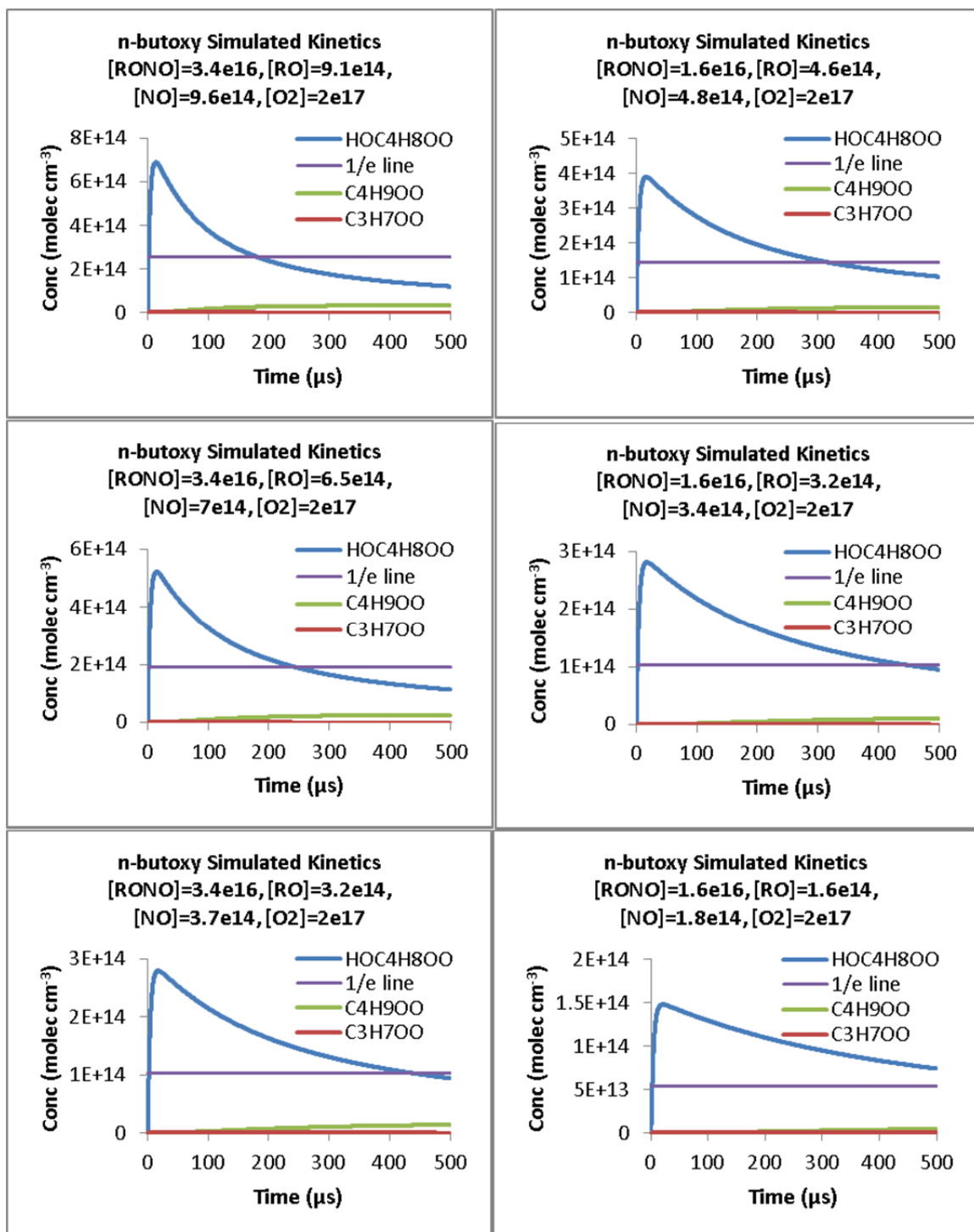


Figure 10.3 Kinetics simulations of HOC₄H₈OO• and peroxy species for our alkoxy experiments, 0–500 μs after C₄H₉O• formation. Various [RONO] and photolysis ratios were used (see individual plots for details). For all experiments, [O₂] = 2 × 10¹⁷ molec cm⁻³, *p* = 300 torr. The lifetime of HOC₄H₈OO• is indicated by the intersection of the kinetics trace (blue line) with the 1/e concentration (purple line). The lifetimes are in good agreement with our experiment (Figure 10.2).

Determination of the Relative Rate Constant $k_{\text{isom}}/k_{\text{O}_2}$

The main goals of the study presented in this chapter were to measure the A-X electronic spectrum of $\text{HOC}_4\text{H}_8\text{OO}\cdot$ and direct kinetics of $\text{HOC}_4\text{H}_8\text{OO}\cdot$ destruction. To date, limited relative kinetics data have been obtained. The reported $k_{\text{isom}}/k_{\text{O}_2}$ should be considered preliminary.

As described in the *Introduction* section, the relative rate constants of the isomerization channel (Reaction 10.2) and the O_2 channel (Reaction 10.3) can be determined by varying $[\text{O}_2]$ and measuring the absorptions of $\text{HOC}_4\text{H}_8\text{OO}\cdot$. $k_{\text{isom}}/k_{\text{O}_2}$ can be extracted by measuring the absorbance (A) relative to “[O_2] = 0” (A_0), then applying Equations 10.10–10.13.

There are two items of note for our relative kinetics experiment. First, at $[\text{O}_2] = 0$, we do not form any $\text{HOROO}\cdot$, and any absorbance measurements that we make are meaningless. We therefore define A_0 as the y-intercept of the regression line fit to the rest of the absorbance data (same procedure as used in our ν_1 experiment in Chapter 8). Second, we are using a much higher $[\text{RO}\cdot]$ than in the ν_1 experiment, and therefore a much higher $[\text{NO}]$. Consequently, the correction factors X_{kin} and X_{prompt} will not be the same as in Chapter 8, and will be recalculated here.

To determine $k_{\text{isom}}/k_{\text{O}_2}$, A_0/A was measured at the largest peak of the A-X spectrum, 7556 cm^{-1} , for the range $2 \times 10^{17}\text{ molec cm}^{-3} < [\text{O}_2] < 8 \times 10^{18}\text{ molec cm}^{-3}$. The peak was measured 10 μs after photolysis to ensure that $\text{HOC}_4\text{H}_8\text{OO}\cdot$ was not being destroyed, as shown in the *Kinetics* section above. 800 ringdown traces, or 80 seconds of data, were averaged for each $[\text{O}_2]$ concentration (16 shots per point, 50 data points). The resulting absorbances were then scaled to $[\text{C}_4\text{H}_9\text{ONO}]$ concentration by scaling to the gas

flows and pressure in the CRDS cell. We then used Equations 10.10–10.13 to determine $k_{\text{isom}}/k_{\text{O}_2}$.

Figure 10.4 shows the plot of A_0/A vs $[\text{O}_2]$ for *n*-butoxy, measured using the A-X spectrum peak at 7556 cm^{-1} . The linear fit is reasonable given the low number of data points taken ($R^2 = 90.4\%$). With 2σ errors, the slope of the plot is $(6.3 \pm 2.1) \times 10^{-20}\text{ cm}^{-3}$ and the intercept is (1.00 ± 0.08) .

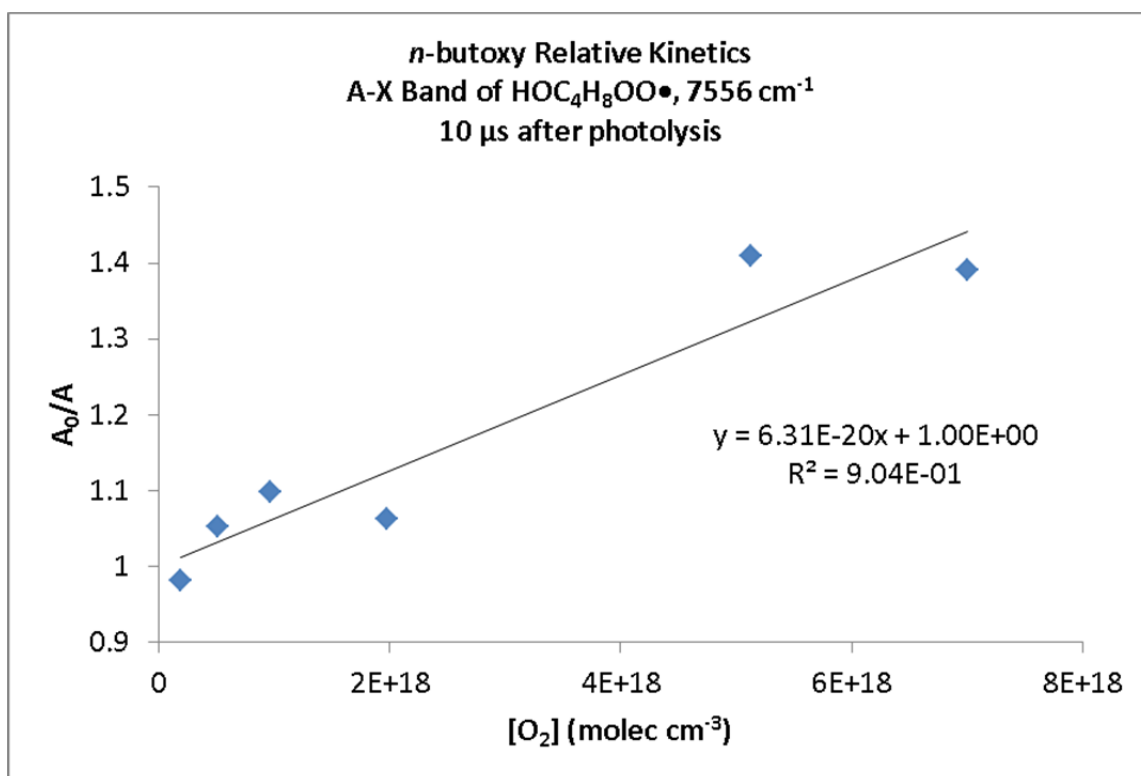


Figure 10.4. Plot of A_0/A vs $[\text{O}_2]$ for *n*-butoxy as measured by the A-X electronic spectrum peak of $\delta\text{-HOC}_4\text{H}_8\text{OO}\bullet$ at 7556 cm^{-1} . With 2σ errors, this plot has a slope of $(6.3 \pm 2.1) \times 10^{-20}\text{ cm}^3$, and an intercept of (1.00 ± 0.08) . Including the correction factor $X = (0.88 \pm 0.05)$, the resulting $k_{\text{isom}}/k_{\text{O}_2}$ value for *n*-butoxy is determined to be $(1.39 \pm 0.47) \times 10^{19}\text{ cm}^{-3}$, with 2σ error.

As noted earlier, we must recalculate the correction factors X_{kin} and X_{prompt} (Equations 10.12 and 10.13) with our elevated NO ($6.8 \times 10^{14}\text{ molec cm}^{-3}$). This [NO] is the sum of the calculated $[\text{RO}\bullet]$ (Table 10.1) and the additional NO present in the *n*-butyl

nitrite (see the *FTIR* section for more information). The relevant parameters and derived values of X_{kin} , X_{prompt} , and the overall correction factor X_{tot} are summarized in Table 10.5.

Our results show that $X_{\text{kin}} = 0.92 \pm 0.05$, $X_{\text{prompt}} = 0.96 \pm 0.02$, and $X_{\text{tot}} = 0.88 \pm 0.05$ (2σ).

Using this correction factor and our A_0/A , we obtain $k_{\text{isom}}/k_{\text{O}_2} = (1.39 \pm 0.47) \times 10^{19} \text{ cm}^{-3}$.

Table 10.5. Parameters used for calculation of correction factors and $k_{\text{isom}}/k_{\text{O}_2}$ for A-X band

	Units	Best Value	Uncertainty (2σ)
$\left[\left(\frac{\partial \left(\frac{A_0}{A} \right)}{\partial [\text{O}_2]} \right)_{[\text{O}_2]=0} \right]^{-1}$	10^{19} cm^{-3}	1.58	0.53
$k_{\text{decomp}}/k_{\text{isom}}$		0.0024	0.0017
$k_{\text{NO}}[\text{NO}]/k_{\text{isom}}$		0.0262	0.0187
ϕ_{pi}		0.038	0.018
X_{kin}		0.92	0.05
X_{prompt}		0.96	0.02
$X_{\text{kin}} \times X_{\text{prompt}}$		0.88	0.05
$k_{\text{isom}}/k_{\text{O}_2}$	10^{19} cm^{-3}	1.39	0.47

Table 10.6 contains a summary of the relative rate constants $k_{\text{isom}}/k_{\text{O}_2}$ for *n*-butoxy found in the literature and compares our value measured from the A-X band. We observe that the preliminary value of $k_{\text{isom}}/k_{\text{O}_2}$ as determined from the A-X band is in good agreement with all of the previous studies in the literature, although subject to somewhat large uncertainty (34%) compared to our ν_1 CRDS experiment from Chapter 8 (9%).

Table 10.6. Comparison of relative rate constant determinations $k_{\text{isom}}/k_{\text{O}_2}$ and derived k_{isom} for *n*-butoxy and 2-pentoxy

	$k_{\text{isom}}/k_{\text{O}_2}$ (10^{19} cm^{-3}) ^a	k_{isom} (10^5 s^{-1}) ^b	Molecules detected	Method	<i>P</i> (<i>torr</i>)	Ref
<i>n</i> -butoxy	1.39 ± 0.47	2.0 ± 1.2	δ -hydroxy- <i>n</i> -butyl peroxy	Slow flow, CRDS (A-X)	330	This work
	1.96 ± 0.25	2.7 ± 1.4	δ -hydroxy- <i>n</i> -butyl peroxy	Slow flow, CRDS (OH Str)	330	Chapter 7
	1.69 ± 0.15	2.4 ± 1.2	δ -hydroxy- <i>n</i> -butyl peroxy	Slow flow, CRDS (OH Str)	670	Chapter 8
	2.0 ± 0.4	2.7 ± 1.5	Butyl nitrite, Butanal,	Static, FTIR	700	Cassanelli ¹⁵⁵
	1.5 ± 0.4	2.1 ± 1.2	4-hydroxy butanal	Static, GC	760	Cox ¹⁵⁶
	1.9 ± 0.4	2.7 ± 1.4	Butane, Butanal	Static, FTIR	700	Niki ¹⁴⁸
	2.1 ± 0.5	2.9 ± 1.6	Butyl nitrite, Butanal	Slow flow, GC	760	Cassanelli ¹⁶⁰
	1.8 ± 1.1	2.5 ± 2.0	Butyl nitrite, Butanal	Slow flow, GC	760	Cassanelli ¹⁶⁰
	1.8 ± 0.6	2.5 ± 1.5	Butane, Butanal	Static, FTIR	760	Geiger ¹⁶¹
	0.25 ± 0.19^c	0.35 ± 0.20^c	Butanal, 4-hydroxy butanal	Fast flow, LIF	38	Hein ¹⁵⁹
	1.6	2.2	OH and NO ₂	Static, GC	740	Carter ¹⁵⁴
	2.1 ± 1.8^d	2.9 ± 1.4^d		Recommendation	760	IUPAC ¹¹⁸

a) All uncertainties are 2σ . All studies other than the current work treat all alkoxy reactions besides isomerization and reaction with O₂ as negligible.

b) Computed k_{isom} assuming literature value of $k_{\text{O}_2} = (1.4 \pm 0.7) \times 10^{-14} \text{ cm}^3 \text{ s}^{-1}$ for *n*-butoxy.²⁸

c) Unlike the other studies, Hein directly measured k_{isom} . In this table, we calculate the ratio $k_{\text{isom}}/k_{\text{O}_2}$ from Hein's measurement using the literature value of k_{O_2} .

d) The IUPAC recommendation for $k_{\text{isom}}/k_{\text{O}_2}$ is computed from their individual recommendations of the isomerization and O₂ reactions

FTIR Analysis of *n*-butyl nitrite

Four samples of *n*-butyl nitrite were measured in the FTIR, and will be presented in order of decreasing purification (fresh and freeze pumped, fresh but not freeze pumped, old but not freeze pumped, and old but stored at room temperature).

Figure 10.5 shows the FTIR spectrum for the purest sample: a freshly opened bottle of butyl nitrite from Sigma-Aldrich, stored at 4 °C, and freeze pumped 3 times prior to use. Three FTIR spectra were taken of this sample: the first spectrum with 148 torr of butyl nitrite, the second spectrum with 62 torr, and the third spectrum of 78 torr. Time was allowed to pass between when the FTIR spectra were taken: the second

spectrum was taken 15 minutes after the first, and the third was taken 45 minutes after the first.

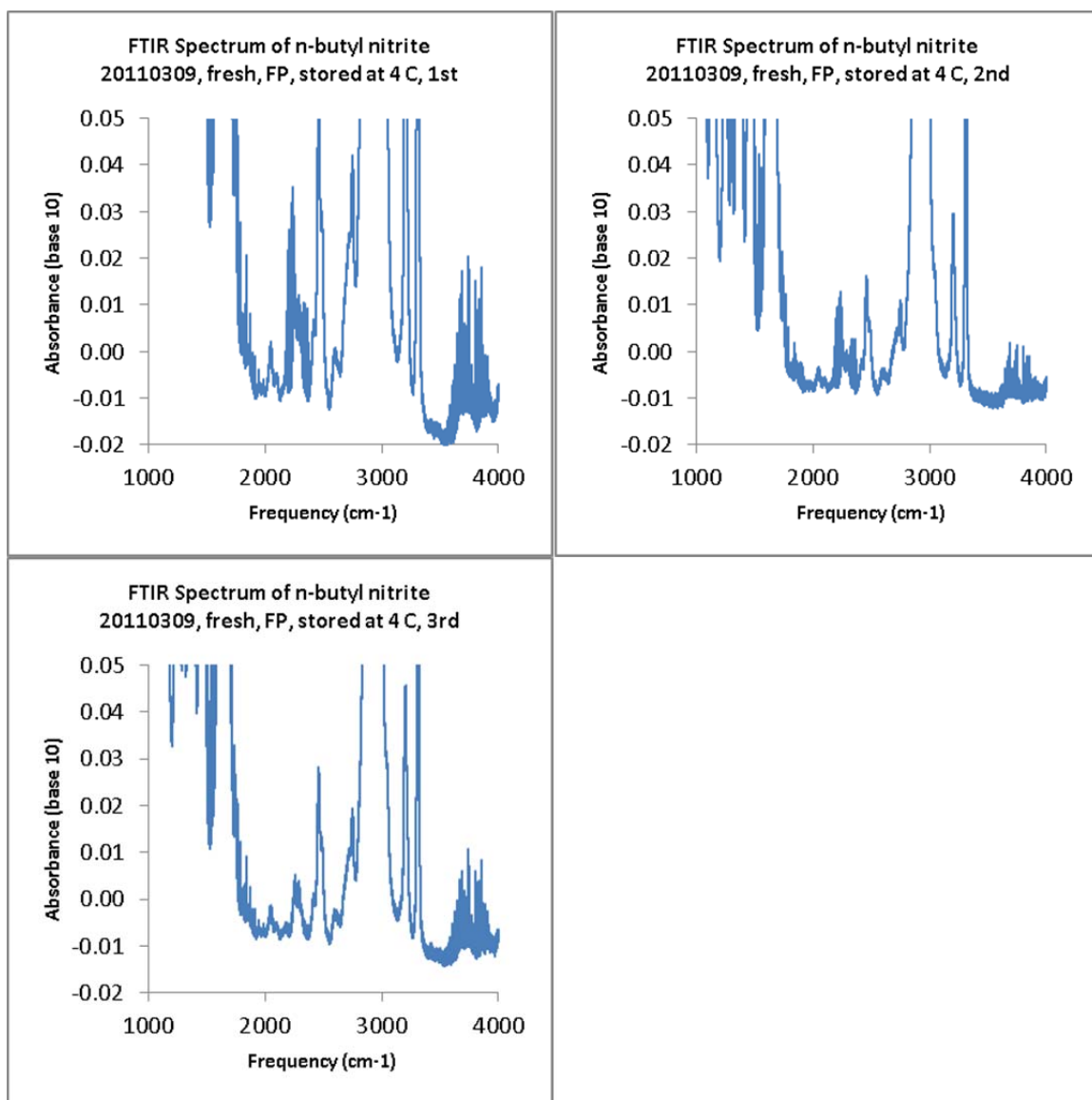


Figure 10.5. FTIR Spectra of *n*-butyl nitrite (March 2011 sample). The butyl nitrite was a freshly opened sample from Aldrich, stored at 4 °C, and freeze pumped 3 times prior to use. Part a (upper left): first spectrum (148 torr). Part b (upper right): second spectrum (62 torr), 15 minutes after first sample. Part c (lower left): third spectrum (78 torr), 45 minutes after first sample.

The spectra in Figure 10.5 show peaks that vary in height as a function of the pressure in the FTIR cell (and therefore the amount of sample injected). These are the

peaks at 1600 cm^{-1} (RONO), 2050 cm^{-1} , 2350 cm^{-1} (CO_2), 2970 cm^{-1} (RONO), and 3860 cm^{-1} (CO_2). There is also a peak at 2315 cm^{-1} that is present in the first two spectra, but not in the third.

Figure 10.6 shows the NO band region for all three spectra that were taken (centered at 1875 cm^{-1}). Weak NO peaks are observed in the first spectrum, much stronger NO lines are observed in the second spectrum and much weaker peaks are observed in the third spectrum. No purification was performed between the scans: it appears that $[\text{NO}]$ is varying over time.

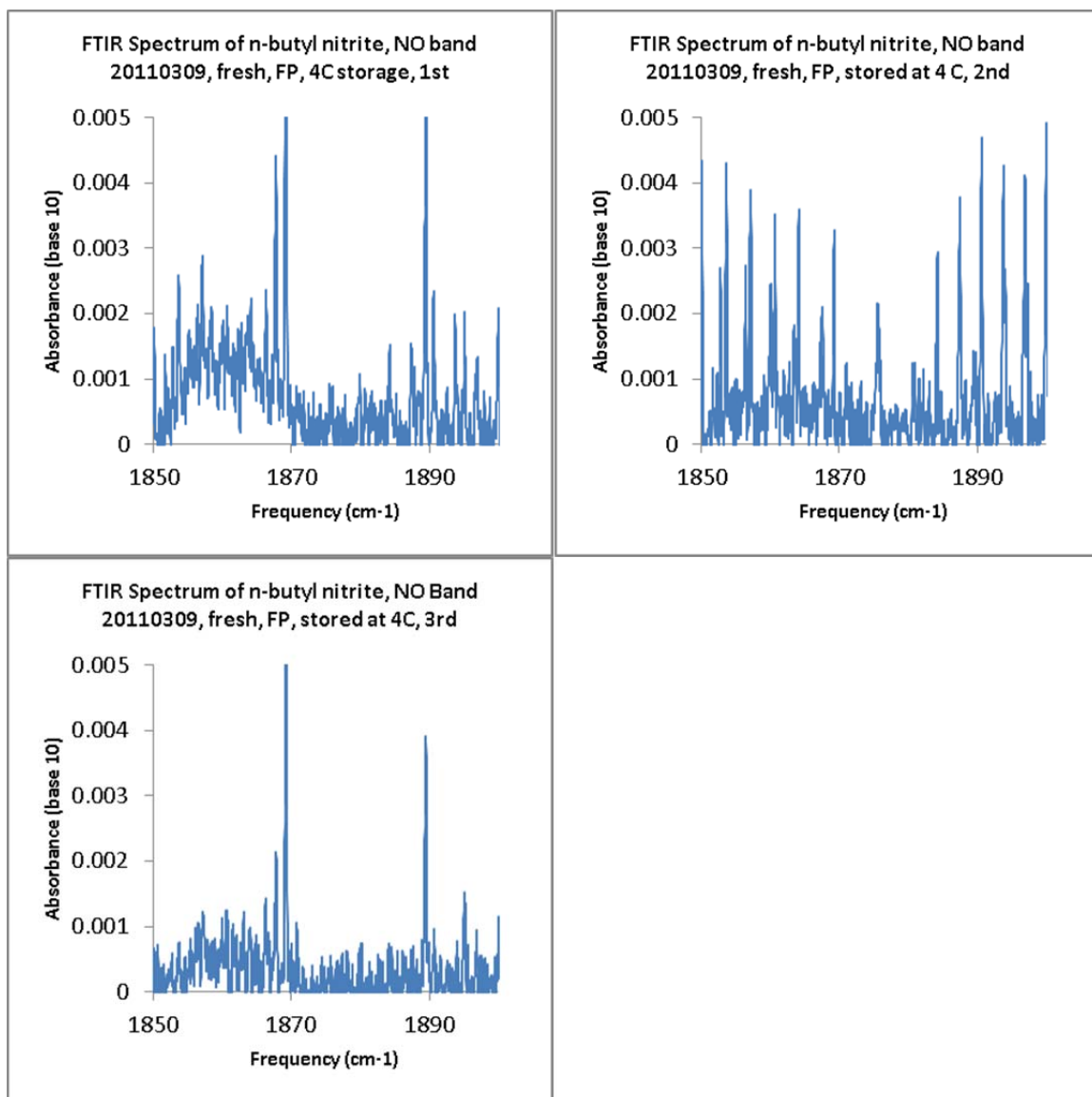


Figure 10.6. FTIR Spectra of the NO vibrational band region of *n*-butyl nitrite. The butyl nitrite was a freshly opened sample from Aldrich, stored at 4 °C, and freeze pumped 3 times prior to use. Part a (upper left): first spectrum (148 torr). Part b (upper right): second spectrum (62 torr), 15 minutes later. Part c (lower left): third spectrum (78 torr), 45 minutes after first sample.

The FTIR spectra of the other three samples and their associated NO bands are shown in Figures 10.7 and 10.8, with Figure 10.7 representing a purer sample than the ones presented in Figure 10.8. The second sample (Figure 10.7) was the same freshly opened butyl nitrite as the first sample discussed above, but not freeze pumped (besides

pumping the atmosphere off prior to FTIR injection). Two FTIR spectra of this sample were taken, 10 minutes apart. The third sample (Figure 10.8, top) was a 4 week old sample of butyl nitrite stored at 4 °C, not freeze pumped prior to measurement. The fourth sample (Figure 10.8, bottom) was an 8 week old sample of butyl nitrite stored at 25 °C, measured to assess the effects of decomposition.

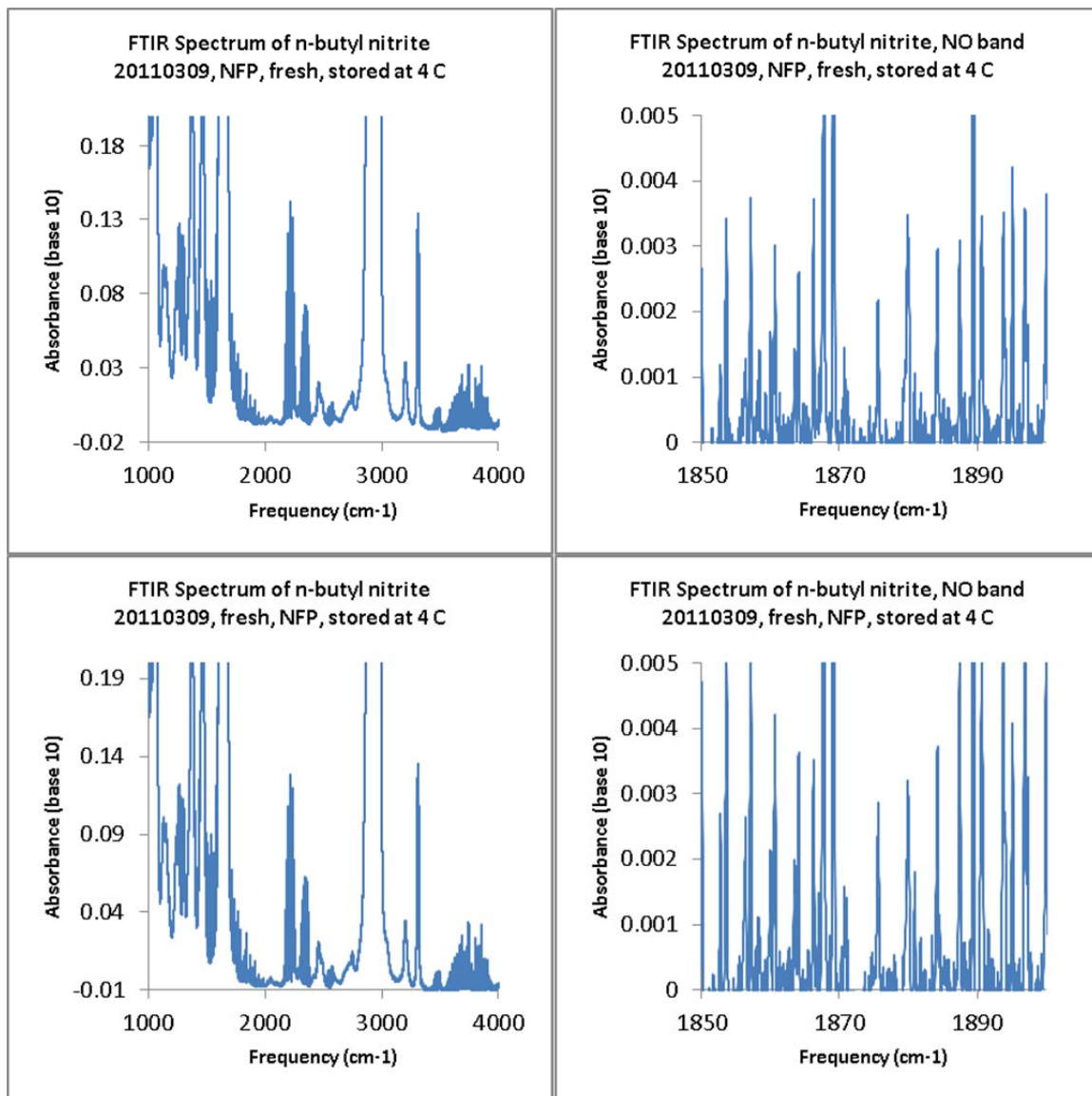


Figure 10.7. FTIR spectra of the full scan and NO vibrational band region of *n*-butyl nitrite. The butyl nitrite was a freshly opened sample from Aldrich, stored at 4 °C, and not freeze pumped. Part a (upper left): first spectrum (68 torr), full range. Part b (upper right): first spectrum (68 torr), NO band. Part c (lower left): second spectrum (66 torr), 10 minutes after first sample, full range. Part d (lower right): second spectrum (66 torr), NO band.

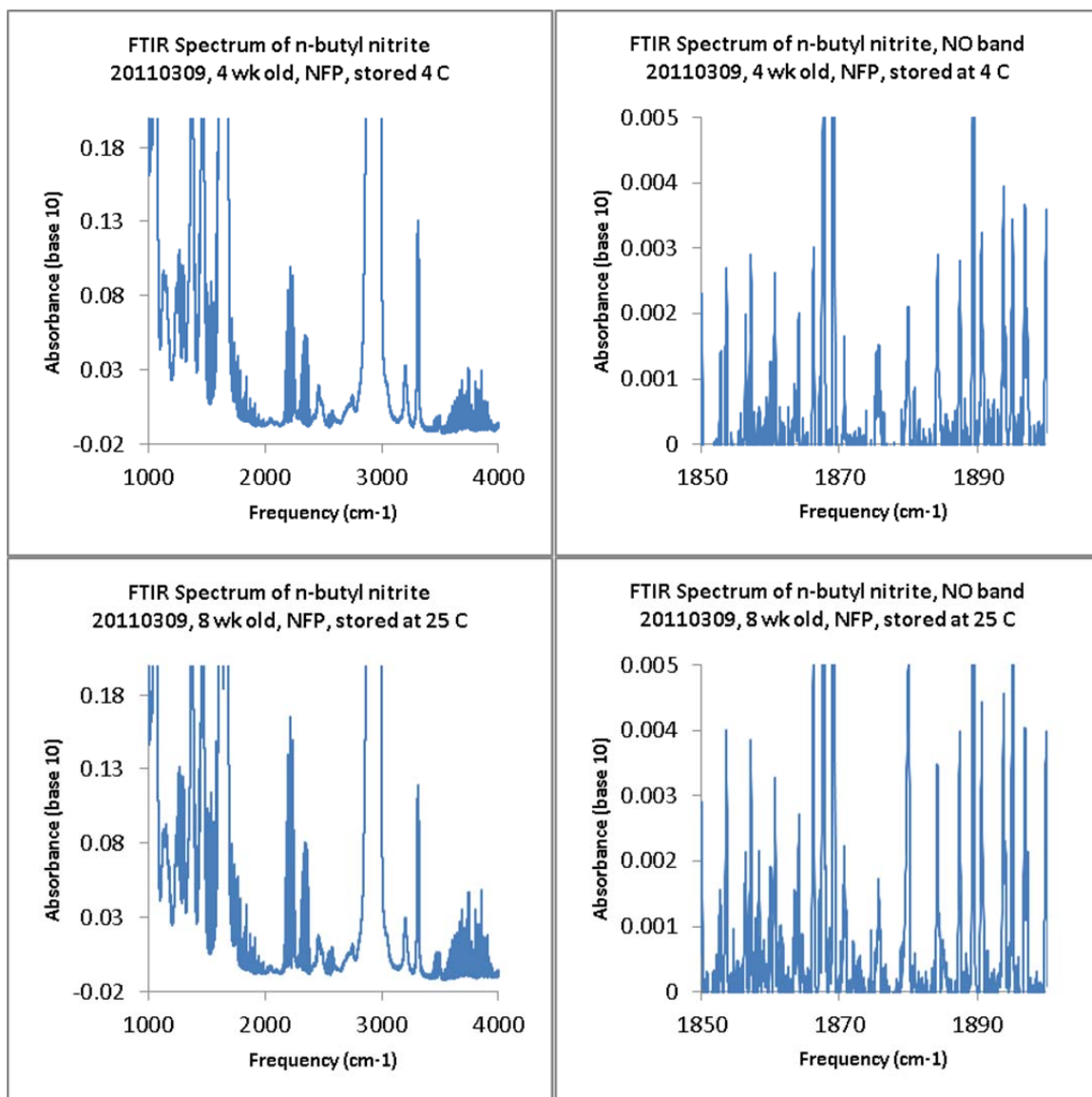


Figure 10.8. FTIR spectra of the full scan and NO vibrational band region of *n*-butyl nitrite. Part a (upper left): 4 week old sample stored at 4 °C, not freeze pumped prior to measurement (65 torr), full range. Part b (upper right): same as part a, NO band. Part c (lower left): 8 week old sample stored at room temperature, not freeze pumped prior to measurement (65 torr), full range. Part d (lower right): same as part c, NO band.

With the FTIR spectra from each sample recorded, we can now fit the PNNL reference spectrum of NO to each *n*-butyl nitrite spectrum. Figure 10.9 shows the fitting to the NO band for the three spectra taken for the first sample (fresh nitrite, freeze pumped, stored at 4 °C). The other three samples had NO bands most similar to the

second spectrum of the first sample (Figure 10.9b), and thus their fits will not be shown here.

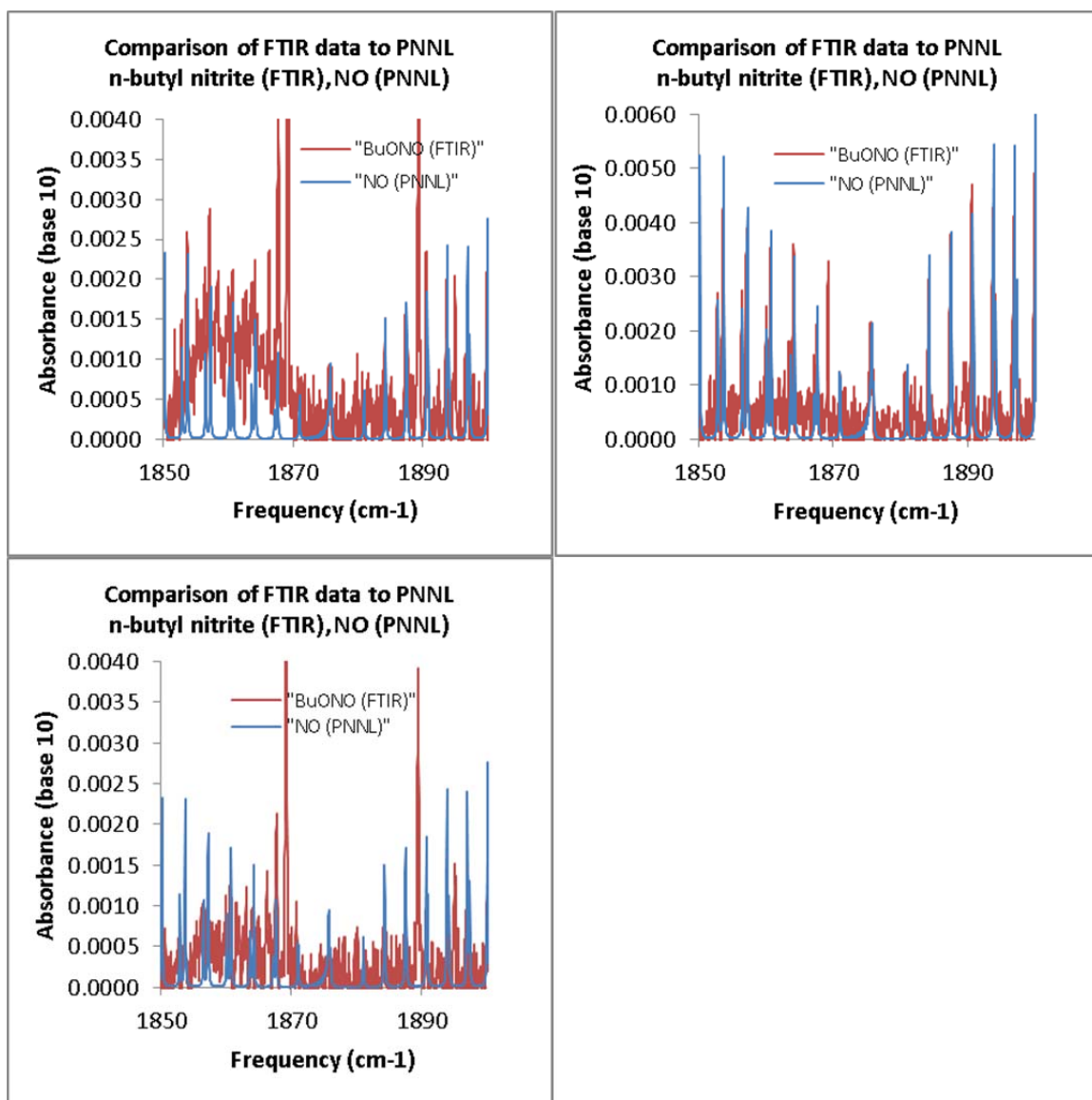


Figure 10.9. FTIR spectra of the NO bands in *n*-butyl nitrite (March 2011 sample, freshly opened, freeze pumped, stored at 4 °C) compared to PNNL reference spectra of NO. Part a (upper left): first spectrum taken (PNNL scaled by a factor of 4). Part b (upper right): second spectrum taken (15 minutes after first, PNNL scaled by a factor of 9). Part c (lower left): third spectrum taken (45 minutes after first, PNNL scaled by a factor of 4).

The fit of the PNNL reference band to the FTIR band in Figure 10.9b is good. However, the fits in Figures 10.9a and 10.9c show inconsistencies between fitting the P

and R branches. The peak ratios in the experimental spectrum do not match the peak ratios in the reference spectrum, leading to extra uncertainty on the amount of NO present in the cell. Additionally, the FTIR instrument was not able to produce a totally correct baseline for any of the spectra. Despite best efforts to manually produce better baselines, inconsistencies still appear in regions of the spectra (in this case, between 1850 and 1870 cm^{-1}). It is also possible that there is an absorber in this region, although it appears to vary inversely with the amount of NO present. Despite these problems, best estimates of [NO] were made, with the stipulation that all reported [NO] values should have around a factor of 5 uncertainty.

Finally, the concentration of $\text{C}_4\text{H}_9\text{ONO}$ was determined by measuring the ON-O stretch peak (1575–1725 cm^{-1}) and comparing to the integrated absorbance calculated in Chapter 7 ($I_{\text{base e}} = 194 \text{ km mol}^{-1}$, or $3.22 \times 10^{-17} \text{ cm molec}^{-1}$). This corresponds to a cross section in the FTIR of $I_{\text{base10}} = 84.2 \text{ km mol}^{-1}$, or $1.4 \times 10^{-17} \text{ cm molec}^{-1}$. The largest peak at 1670 cm^{-1} is very strong, and perhaps in the non-linear absorption region (shown in Figure 10.10), causing us to underestimate [RONO]. Thus, the NO contamination that we report is an upper limit.

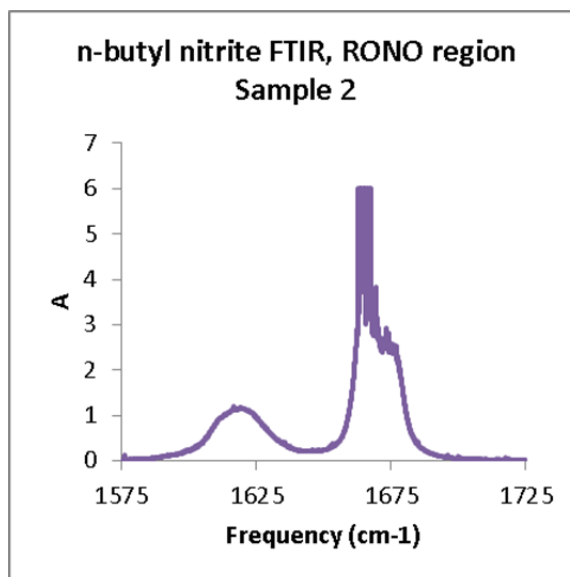


Figure 10.10. – Sample ON-O stretch spectrum (FTIR) of *n*-butyl nitrite. For this sample, the integrated absorbance is 92.7 cm^{-1} , or $[\text{RONO}] = 3.5 \times 10^{17} \text{ molec cm}^{-3}$.

We can determine $[\text{NO}]$ in the CRDS experiment based on the FTIR spectra by using the following procedure. All reference spectra reported by PNNL are scaled by the authors to an effective burden ($[\text{gas}] \times \text{path length}$) of $2.48 \times 10^{15} \text{ molec cm}^{-2}$. $[\text{NO}] \times \text{path length}$ in the experimental FTIR spectrum was calculated by scaling the PNNL NO spectrum to the NO vibrational band at 1875 cm^{-1} , then multiplying the scaling factor by $2.48 \times 10^{15} \text{ molec cm}^{-2}$. Dividing by the FTIR path length (19 cm) gives us $[\text{NO}]$.

The *n*-butyl nitrite sample descriptions, FTIR conditions, scaling factors of the reference spectra to the FTIR spectra, and calculated $[\text{NO}]$ in the CRDS experiment are summarized in Table 10.7. Our FTIR data suggest that using a freeze pumped sample of butyl nitrite will yield excess $[\text{NO}]_{\text{CRDS}} = (0.3\text{--}1) \times 10^{14} \text{ molec cm}^{-3}$, and that not freeze pumping the sample (regardless of storage conditions) will yield excess $[\text{NO}]_{\text{CRDS}} = (1\text{--}2) \times 10^{14} \text{ molec cm}^{-3}$. The values reported from this study have large uncertainties associated with them due to inconsistencies in the measured NO bands and nonlinearities

in the RONO spectrum. The derived excess $[\text{NO}]_{\text{CRDS}}$ should be considered an upper limit, and may be high by a factor of 2–5.

Based on the FTIR analysis, we expect that the extra $[\text{NO}]$ introduced from the nitrite sample itself is 5%-10% of the $[\text{NO}]$ generated from the nitrite photolysis (Reactions 10.1 and 10.2).

Table 10.7. Scale factors for FTIR and PNNL spectra and determination of $[\text{NO}]$ in the CRDS experiment

	Units	1	1a	1b	2	2a	3	4
Sample Age		Fresh	Fresh	Fresh	Fresh	Fresh	4 wks.	8 wks.
Storage Temp	K	277	277	277	277	277	277	293
Freeze Pump?		yes	yes	yes	no	no	no	no
Pressure	torr	148	62	77	68	66	65	65
$[\text{RONO}]$ (by ON-O str, 1575-1725 cm^{-1})	molec cm^{-3}	8.6×10^{17}	4.4×10^{17}	6.0×10^{17}	5.1×10^{17}	5.1×10^{17}	5.1×10^{17}	4.5×10^{17}
NO scale factor (FTIR/PNNL)		4	9	4	10	12	7	8
$[\text{NO}]_{\text{FTIR}}$	molec cm^{-3}	6.6×10^{14}	1.5×10^{15}	6.6×10^{14}	1.7×10^{15}	2.0×10^{15}	1.2×10^{15}	1.3×10^{15}
$[\text{RONO}]:[\text{NO}]$		1300	290	910	300	250	420	350
$[\text{NO}]_{\text{CRDS}}$	molec cm^{-3}	3.3×10^{13}	1.4×10^{14}	4.7×10^{13}	1.4×10^{14}	1.7×10^{14}	9.7×10^{13}	1.3×10^{14}

Discussion

Measuring the A-X Spectrum of $\delta\text{-HO-1-C}_5\text{H}_{10}\text{OO}\cdot$

Given the studies in Chapters 7 and 8, the next logical extension of the alkoxy A-X spectroscopy studies would be the product of 2-pentoxy isomerization: $\delta\text{-HO-1-C}_5\text{H}_{10}\text{OO}\cdot$. Unfortunately, such a study would be complicated by prompt decomposition and the large decomposition rate of 2-pentoxy ($k_{\text{decomp}} = 2 \times 10^4 \text{ s}^{-1}$)¹¹⁷ compared to isomerization ($k_{\text{isom}} = 2.7 \times 10^5 \text{ s}^{-1}$, Chapter 8). Since decomposition (Reactions 10.6 and 10.9) will lead to the formation of other peroxy radicals, the

observed spectrum will be a mixture of δ -HO-1-C₅H₁₀OO• and the decomposition product C₃H₇OO•.

To determine the extent of this interference, we modeled the kinetics of the 2-pentoxy system using the same parameters (k_{isom} , k_{O_2} , k_{decomp}) as in Chapter 8. We used the same chemical concentrations as for the A-X spectrum of *n*-butoxy in Figure 10.1 ($[\text{RONO}] = 3.4 \times 10^{16}$ molec cm⁻³, $[\text{RO}\cdot] = 6.5 \times 10^{14}$ molec cm⁻³, $[\text{NO}] = 7.0 \times 10^{14}$ molec cm⁻³, $[\text{O}_2] = 2 \times 10^{17}$ molec cm⁻³). The simulation is shown in Figure 10.11.

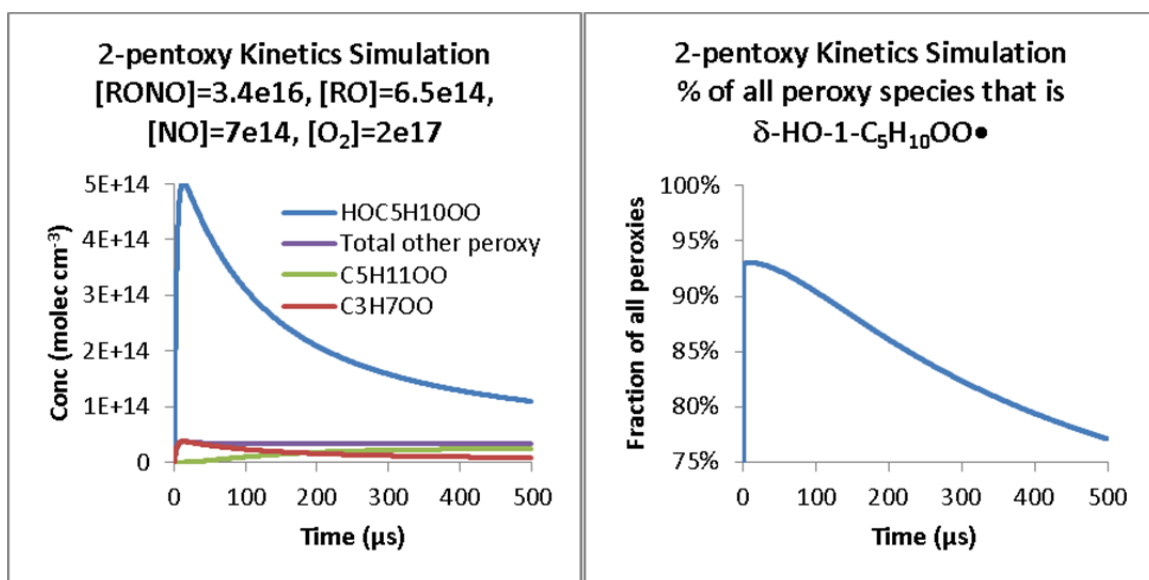


Figure 10.11. Kinetics simulations for 2-pentoxy system: concentrations of peroxy species and fraction of peroxies that are the isomerization product δ -HO-1-C₅H₁₀OO•, 0–500 μ s after 2-pentoxy formation (chemical concentrations listed on the plot). Over 0–500 μ s, 7%–20% of the peroxy species belong to non-isomerization products.

The isomerization product δ -HO-1-C₅H₁₀OO• reaches its maximum concentration 15 μ s after alkoxy formation. We note that even within this short timescale, the decomposition product C₃H₇OO• forms in appreciable quantities, 7% of the total peroxy species in the system. (In the *n*-butoxy system, we expected less than 1%) At later times,

we observe formation of $C_5H_{11}OO\cdot$ while $\delta\text{-HO-1-C}_5\text{H}_{10}OO\cdot$ is destroyed, causing the spectrum to become contaminated. At 500 μs , over 20% of the peroxy species are products other than the alkoxy isomerization product.

The overall conclusion is that the A-X spectrum of $\delta\text{-HO-1-C}_5\text{H}_{10}OO\cdot$ obtained from alkoxy chemistry will be contaminated by other peroxy species. Since decomposition is temperature dependent, it is likely that reducing the temperature of the CRDS cell will allow for purer A-X spectra to be obtained.¹¹⁷ Room temperature experiments must contain the caveat that other peroxy species are contributing to the reported spectrum.

Conclusions

In this chapter, we have reported the first clean A-X electronic spectrum of the primary product of *n*-butoxy isomerization in the presence of oxygen: $\delta\text{-HOC}_4\text{H}_8OO\cdot$. The spectrum is similar in shape and intensity to *n*-butyl peroxy: a broad absorption in the near-IR with three features in the range 7200-7700 cm^{-1} . The relative intensities of these three features are different between $\delta\text{-HOC}_4\text{H}_8OO\cdot$ and *n*- $C_4H_9OO\cdot$. Under our experimental conditions, the recorded spectrum is expected to be at least 99% $\delta\text{-HOC}_4\text{H}_8OO\cdot$. We can measure the kinetics of $\delta\text{-HOC}_4\text{H}_8OO\cdot$ directly using the A-X band, observing $\delta\text{-HOC}_4\text{H}_8OO\cdot$ of 200–400 μs , in agreement with kinetics modeling. We have shown that the A-X band can be used for measurement of alkoxy relative kinetics, and obtain a preliminary k_{isom}/k_{O_2} , $(1.39 \pm 0.47) \times 10^{19} \text{ cm}^{-3}$, in agreement with the CRDS study in Chapter 8 (ν_1 band). Finally, we have assessed the purity of the *n*-butyl

nitrite used in our alkoxy experiments, and have shown that the [NO] contributed from the *n*-butyl nitrite sample is 5%–10% of the NO generated from alkyl nitrite photolysis.

Acknowledgements

We thank Ralph H. Page for improvements to the optical setup and assistance with experiments, and Nathan C. Eddingsaas for assistance with acquiring the FTIR spectrum of *n*-butyl nitrite. The experiments performed in this chapter were funded under NASA Upper Atmosphere Research Program Grant NNX09AE21G2.